Original

Chen, Y.; Angelova, A.; Angelov, B.; Drechsler, M.; Haramus, V.M.;
Willumeit-Roemer, R.; Zou, A.:

Sterically stabilized spongosomes for multidrug delivery of anticancer nanomedicines

In: Journal of Materials Chemistry B (2015) Royal Society of Chemistry

DOI: 10.1039/c5tb01193k

Journal of Materials Chemistry B

PAPER

View Article Online
View Journal | View Issue

Cite this: J. Mater. Chem. B, 2015, 3, 7734

Sterically stabilized spongosomes for multidrug delivery of anticancer nanomedicines

Yiyin Chen,†[a] Angelina Angelova,†[b] Borislav Angelov,[c] Markus Drechsler,[d] Vasil M. Garamus,[e] Regine Willumeit-Römer[e] and Aihua Zou*[a]

Received 23rd June 2015,
Accepted 10th August 2015

DOI: 10.1039/c5tb01193k

www.rsc.org/MaterialsB

Multidrug delivery devices are designed to take advantage of the synergistic effects of anticancer agents in combination therapies. Here we report novel liquid crystalline self-assembled nanocarriers enhancing the activity of the phytochemical anticancer agent baicalin (BAI) in combination with *Brucea javanica* oil (BJO), which ensures safe formulations for clinical applications. Small-angle X-ray scattering (SAXS) and cryogenic transmission electron microscopy (cryo-TEM) evidenced the multicompartment, sponge-type nano-organization of the blank and multidrug-loaded liquid crystalline carriers. Physico-chemical stability of the sponge nanoparticles was achieved through PEGylation of the lipid membranes, which make up the drug nanocarriers. The proposed green nanotechnology for nanocarrier preparation by supramolecular self-assembly provided a multidrug encapsulation efficiency as high as 75%. The apoptosis study with the human lung carcinoma cell line A549 demonstrated improved efficacy of the multidrug delivery nanocarriers in comparison to the single-drug reservoirs. The obtained results evidenced the synergistic anticancer apoptotic effects of the multidrug-loaded nanosponge carriers and suggested the opportunity for *in vivo* translation towards the treatment of lung, gastrointestinal, and ovarian cancers.

Introduction

Liquid crystalline lipid nanocarriers of multicompartment organization, created by self-assembly and nanoarchitectonics principles, have forthcoming applications in various research fields, from theranostic imaging and biosensors in medicine to functional foods, nutraceuticals, and drug delivery systems offering advanced therapeutic innovations.[1–5] The structural advantages[6–9] and enhanced drug encapsulation capacities[10–14] of the liquid crystalline lipid particles attract ongoing interest in the search for nanocarriers that provide minimal side effects in clinical applications such as oncology. In addition, liquid crystalline assemblies generated by functionalized lipid systems display stimulus-responsive properties,[15–19] which permit them to expand the possible therapeutic approaches for the treatment of pathological states.[20–24]

Currently, natural products and phytochemicals attract considerable interest in the development of nanoscale anticancer medicines.[25–32] Patients with cancer have often been at risk of immunocompromise upon treatment with chemotherapeutic drugs.[27d] Owing to the severe side effects observed with some of the potent anticancer agents used in chemotherapy (*e.g.* cardiotoxicity and neural toxicity), new controlled delivery systems need to be elaborated towards more efficient nanodrug design.[33–36]

The flavonoid baicalin (BAI) (Fig. 1) is a single, active compound extracted from *Scutellaria baicalensis*, a herb that has widespread biological functions including anticancer, antibacterial, anti-inflammatory, antioxidant, anti-stress, immunosuppressive and spasmolytic activities.[26] It has been shown that BAI may protect the liver from drug-induced injuries.[28] *Brucea javanica* oil (BJO) is a mixed-oil extract from the nucleoli of *Brucea javanica*. Its oleic and linoleic acid constituents as well as the tetracyclic triterpene quassinoids and anthraquinone exert antitumor activity, especially in lung, liver, ovarian, and cervical cancers.[25b] Among the main bioactive components of BJO, oleic and linoleic acids (Fig. 1) comprise 63.3% and 21.2% of the mass content, respectively,[25a] and have shown synergistic anti-tumor effects.[25c] Importantly, the safety and efficacy profiles of some chemotherapeutic drugs have improved when used in combination with *Brucea javanica* oil. This has resulted in a better immune function and quality of life of the patients with late-stage lung cancer.[27d] Moreover, *Brucea javanica* oil has

[a] East China University of Science and Technology, Shanghai, China. E-mail: aihuazou@ecust.edu.cn
[b] CNRS UMR8612 Institut Galien Paris-Sud, Univ Paris Sud, LabEx LERMIT, Châtenay-Malabry, F-92296 France
[c] Institute of Macromolecular Chemistry, Academy of Sciences of the Czech Republic, Heyrovskeho Nam. 2, 16206 Prague, Czech Republic
[d] Laboratory for Soft Matter Electron Microscopy, Bayreuth Institute of Macromolecular Research (BIMF), University of Bayreuth, D-95440 Bayreuth, Germany
[e] Helmholtz-Zentrum Geesthacht, Centre for Materials and Coastal Research, D-21502 Geesthacht, Germany
† These authors contributed equally to this work.

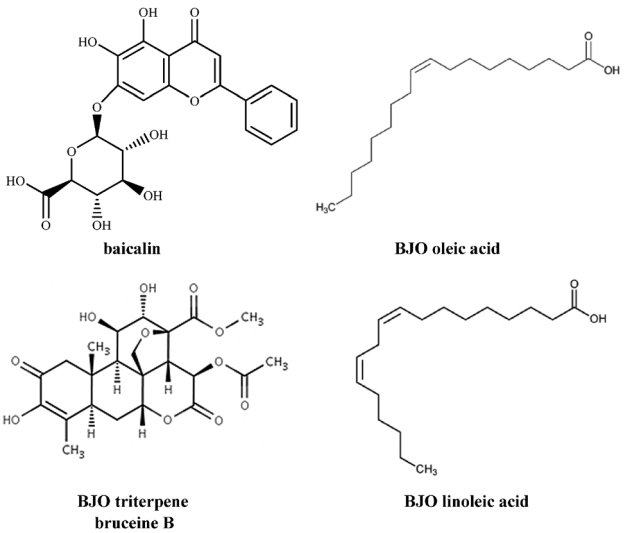

Fig. 1 Chemical structures of the flavonoid baicalin and of the major bioactive components of *Brucea javanica* oil (BJO) used for the preparation of the multidrug-loaded, self-assembled liquid crystalline nanocarriers.

been able to reverse the drug resistance in tumor cells by altering the P-glycoprotein expression in the cell membranes.[27b] Thanks to its low toxicity in clinical applications and various pharmacological activities, BJO may be considered as an attractive ingredient of modern formulations aiming at the treatment of lung, gastrointestinal, ovarian and liver cancers, as well as brain metastasis.[27a,c]

The present study hypothesizes that the joint encapsulation of baicalin (BAI, characterized by strong anti-inflammatory, antioxidant and anticancer properties against pneumonia, lung, and gastrointestinal cancers) and *Brucea javanica* oil (BJO, essential to diminishing the resistance index of drug-resistant cancer cells) in controlled release nanoformulations may ensure the efficacy and safety of combination phyto-chemotherapies. As a matter of fact, co-delivery devices and nanoparticles, allowing for synergistic drug cytotoxicity against diverse cancer cell populations, represent an emerging concept in nanodrug development.[20–24]

The purpose of this work is to design a new nanodelivery system for combination anticancer treatment providing synergistic effects of the chosen anticancer phytochemicals that may target different intracellular signaling pathways. Self-assembled mixtures involving the lyotropic lipid glycerol monooleate (MO) were used to prepare nanosponge-type particles, which were sterically stabilized by a corona of polyethylene glycol (PEG) chains. The amphiphilic compositions were varied towards tuning the sizes of the aqueous and lipid domains in the mesocrystalline structures. High-resolution structural characterization of the nanocarriers was performed by small-angle X-ray scattering (SAXS) and cryogenic transmission electron microscopy (cryo-TEM) imaging. Considering the markedly different solubilities of the BAI and BJO components, a sequential drug release profile from the multicompartment nanocarriers was suggested. Biological evaluation of the multidrug-loaded nanosponge particles was performed with the human lung cancer cell line A549.

Results

Structural organization of the designed nanosponge lipid carriers stabilized by a PEGylated corona

Table 1 presents the compositions of interest for the preparation of liquid crystalline, multicompartment lipid nanocarriers for multidrug loading. Nanocarriers were fabricated based on the phase behavior of the lyotropic lipid glycerol monooleate (MO) and on experiments on the self-assembly of its functionalized mixtures with the polymeric amphiphile polysorbate 80 (P80) in the presence of alginate polymer (alginic acid sodium salt) in aqueous phase. The designed physical agitation schemes (denoted by 1 or 2 for every nanocarrier formulation) aimed at the production of homogeneous aqueous dispersions of liquid crystalline particles with the smallest possible sizes favorable for the cellular uptake of the encapsulated multidrugs. The average particle diameters in the dispersed nanocarrier systems, determined by dynamic light scattering, did not considerably vary as a function of the sequence of applied physical agitations or the mixed amphiphilic compositions (Table 2). A bimodal distribution with peak maxima values in the volume size distribution plot of 61 nm and 310 nm, respectively, was determined for the multidrug-loaded BAI-BJO spongosomes-2. The presence of two kinds of nano-object populations is typical for the monoolein aqueous dispersions and does not result from instability of the nanocarriers. It has been previously shown that small lipid vesicles provide bilayer membrane building blocks for the formation of larger nanoparticles of the inner bicontinuous membrane organization (*e.g.* spongosomes and cubosomes).[1c,5b,6c]

Table 1 Compositions of liquid crystalline nanoparticulate systems of spongosome type, subjected to two physical agitation schemes (1 or 2)[a]

Formulations	GMO (mg)	P80 (mg)	BAI (mg)	BJO (mg)
Blank-spongosome-1[a]	500	66.7	—	—
Blank-spongosome-2[a]	500	66.7	—	—
BAI-spongosome-1	500	66.7	150	—
BAI-spongosome-2	500	66.7	150	—
BAI-BJO-spongosome-2	500	66.7	150	100

[a] The aqueous phase contains 0.5 wt% sodium alginate (PBS buffer pH 7.4). The physical agitation schemes involved cycles of: 1 – high-pressure homogenization step first (5 cycles at 850 bar), then sonication step (15 min in ice bath). 2 – sonication step first (15 min in ice bath), then high-pressure homogenization step (5 cycles at 850 bar).

Table 2 Hydrodynamic nanoparticulate sizes derived from the peak maxima values in the volume distribution plots of dynamic light scattering measurements and zeta potential of freshly prepared spongosome nanocarriers[a]

Samples	Nano-object size (nm)	Zeta potential (mV)
Blank-spongosome-1	74.13	−27.03 ± 1.14
Blank-spongosome-2	60.93	−25.76 ± 0.34
BAI-spongosome-1	63.95	−28.00 ± 1.32
BAI-spongosome-2	52.81	−25.59 ± 1.23
BAI-BJO-spongosome-2	60.93 & 309.99	−31.22 ± 0.89

[a] Measurements at day 1 after samples dispersion; 1 and 2 denote the physical agitation scheme (see Table 1).

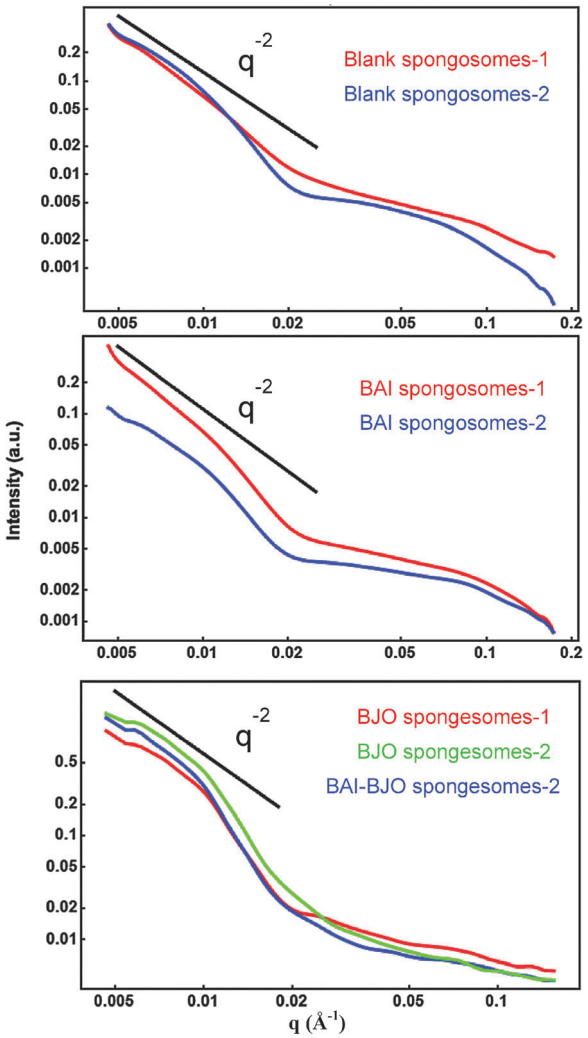

Fig. 2 SAXS patterns of blank and drug-loaded lipid nanocarriers stabilized by polysorbate P80. Top panel: Blank-spongosomes-1 (agitation method 1) and blank-spongosomes-2 nanocarriers (agitation method 2); middle panel: BAI-spongosomes-1 (agitation method 1) and BAI-spongosomes-2 (agitation method 2); bottom panel: BJO-spongosomes-1 (BJO 2 mg mL^{-1}, red plot), BJO-spongosomes-2 (BJO 5 mg mL^{-1}, green plot), and BAI-BJO-spongosomes-2 (agitation method 2, blue plot). The lipid concentration is 10 mg mL^{-1} (MO, glyceryl monooleate), and the drug concentrations are 3 mg mL^{-1} (BAI) and/or 5 mg mL^{-1} (BJO). Aqueous phase: PBS pH 7.4 buffer containing 0.5 wt% sodium alginate.

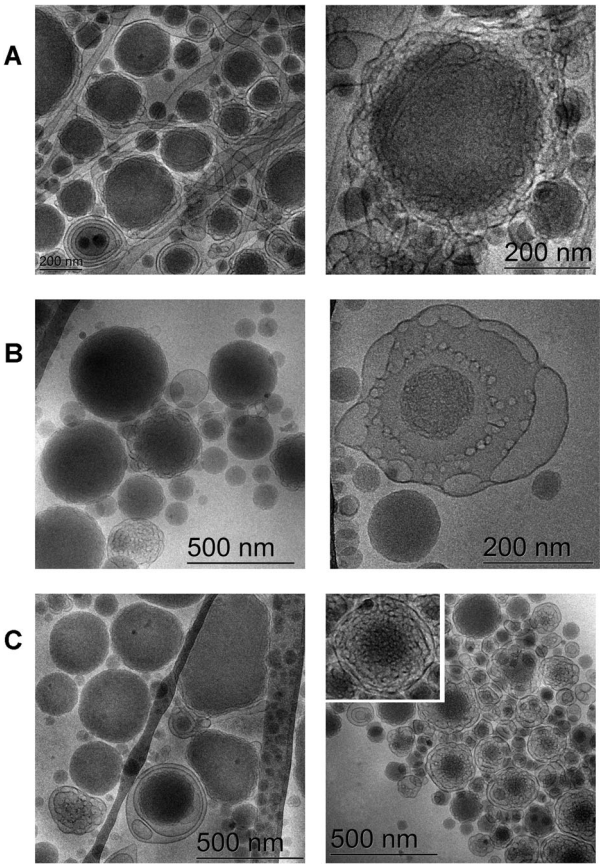

Fig. 3 Cryo-TEM images of blank-spongosomes-2 (A), BAI-spongosomes-2 (B), and BAI-BJO-spongosomes-2 (C). The number 2 denotes the employed agitation method for sample dispersion (method 2), *i.e.* sonication followed by high-pressure homogenization (see Table 1). The lipid concentration is 10 mg mL^{-1} (MO, glyceryl monooleate), and the drug concentration is 3 mg mL^{-1} (BAI) and/or 5 mg mL^{-1} (BJO). Aqueous phase: PBS pH 7.4 buffer containing 0.5 wt% sodium alginate.

Detailed SAXS investigations were performed for the inner organizations of the created amphiphilic nanocarriers dispersed in alginate solution. The obtained SAXS patterns (Fig. 2) demonstrated that the nanocarriers are of liquid crystalline nature and do not display long-range inner crystalline order typical of pure glycerol monooleate assemblies.[1b,6b,7b] Therefore, the internal structure of the P80-stabilized nanoparticles is constituted by sponge lipid membranes rather than by bicontinuous cubic lipid bilayer assemblies. This result was confirmed also by the cryo-TEM data (see Fig. 3 below). The sponge liquid crystalline organization favors the encapsulation of both hydrophobic and hydrophilic therapeutic agents at variance to the traditional drug delivery systems.

SAXS structural analysis revealed that the drug loading in the nanocarriers had a more pronounced influence on the scattering curves of the nanoparticle dispersions as compared to the physical agitation methods. The spongosomes prepared by method 1 and method 2 (Table 1) displayed minor differences in their SAXS curves, *e.g.* blank spongosomes-1 and blank spongosomes-2 (Fig. 2). Fig. 2 demonstrates that the inclusion of BAI in the nanosponge particles does not modify the overall sponge-type nano-organization. This can be attributed to the just-increased contrast of the drug-loaded spongosomes due to higher oxygen content of the BAI molecule. The SAXS data obtained with the BJO-loaded nanocarriers also suggested a high degree of BJO encapsulation in the nanosponges (Fig. 2, bottom panel).

The comparison of the shapes of the scattering curves with scattering of infinite plane ($\sim q^{-2}$) in Fig. 2 indicated that the studied nanocarriers are made up of the core–shell structures. This is consistent with the sponge-type organization of the liquid crystalline nanoparticle cores, which are surrounded by shells of a PEGylated corona of P80 and alginate polymer chains dissolved in the aqueous phase.

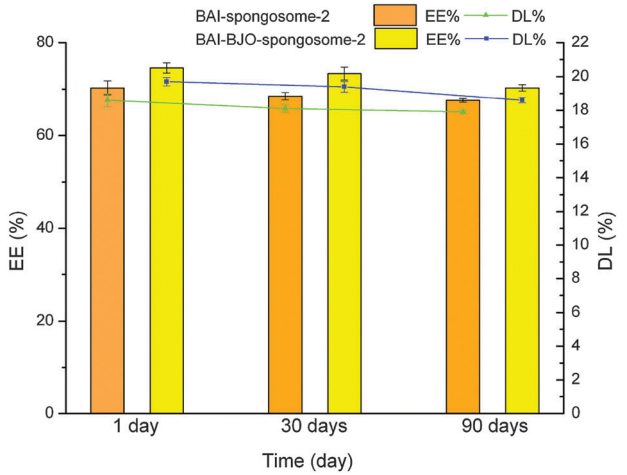

Fig. 4 Values for the entrapment efficiency (EE) and drug loading (DL) determined with nanocarriers at day 1, day 30, and day 90 after preparation. The number 2 denotes the employed agitation method for sample dispersion (see Table 1).

The employed P80 corona stabilization of the nanocarriers ensured their physical stability over prolonged time. This also favored the preservation of the drug encapsulation capacity with time (Fig. 4). It should be noted that no filtering was applied after the physical agitation scheme to prevent the creation of large, self-assembled aggregates. However, such a filtering procedure has been frequently applied in the literature to non-lamellar lipid assemblies dispersed by Pluronic surfactants. Thus, P80 appears to be an efficient stabilizer of the multidrug-loaded nanocarriers in the present work.

The dynamic light scattering data indicated that the nanoparticles present in the aqueous dispersions are characterized by relatively narrow size distributions resulting from the employed vigorous agitation schemes (Table 1). The corresponding maxima in the volume distribution plots, determined by DLS, are given in Table 2. The data suggested that better fragmentation of the lipid mixtures and lower polydispersity of the nano-object system may be obtained by the agitation method 2 involving first a sonication step, followed by high-pressure homogenization. The cryo-TEM imaging and the rest of the nanoparticle evaluations were thus performed with samples produced by method 2.

The performed cryo-TEM investigation evidenced the sponge nano-organization of all nanoparticle preparations in agreement with the above SAXS results. Fig. 3 summarizes typical cryo-TEM images obtained for the blank and the drug-loaded nanocarriers. The dense inner liquid crystalline organization of packed bilayer membranes and a soft corona shell, providing steric stability to the nanoparticles, are readily established by the images. This result fully corroborates the conclusion deduced above from the SAXS investigation. The lack of a crystalline order inside the core of the nanoassemblies confirms their soft matter nature and their sponge-type membrane organization.

Encapsulation efficiency and drug release from nanocarriers

Fig. 4 demonstrates that the encapsulation efficiency (EE) values of baicalin in freshly prepared single drug-loaded nanocarriers (BAI-spongosome-2) and in multidrug-loaded nanocarriers (BAI-BJO-spongosome-2) were 70.3 ± 1.5% and 74.6 ± 1.1%, respectively. The baicalin drug loading (DL) values in the BAI-spongosome-2 and in the BAI-BJO-spongosome-2 were 18.6 ± 0.4% and 19.7 ± 0.2%, respectively. It is interesting to note that the inclusion of BJO in the lipid phase increased the EE and DL of BAI in the spongosome nanocarriers. This may be explained by the affinity of the BAI drug for the lipophilic BJO ingredient or by the structural influence of BJO on the aqueous channel domains of the studied spongosome particles. The latter is consistent with the obtained SAXS results. The enlargement of the spongosomes' water channel sizes should increase the quantity of entrapped BAI. Thus, the encapsulation efficiency of the nanocarriers for BAI is improved in the presence of BJO. No significant changes in the drug loading and drug entrapment efficiencies were observed for all spongosome compositions after 90 days of nanocarrier storage.

The BAI drug release profiles from spongosomes (Fig. 5) were studied *in vitro* in PBS medium (pH 7.4) at 37 °C using the dialysis method with an aqueous bath set on a rotary shaker. BAI release from a free drug suspension was investigated as a control (Fig. 5). During the first 10 h, over 95% of the BAI drug was released from the drug suspension. The accumulative release value reached 100% in the following hours. No drug burst release was observed from BAI-spongosome-2 and BAI-BJO-spongosome-2 nanocarriers, which is consistent with their high encapsulation efficiency. The drug release rate from the spongosome carriers appeared to be markedly reduced, down to about 60–70%, as compared to the drug release from a BAI suspension for the same time period. This demonstrates that the obtained spongosome delivery system is characterized by sustained release behavior for the BAI drug that is liberated through the nanochannel system of the nanocarriers.

The monodrug-loaded (BAI-spongosome-2) and the multidrug-loaded (BAI-BJO-spongosome-2) nanoparticles displayed similar release curves (Fig. 5), which indicates that the co-encapsulation

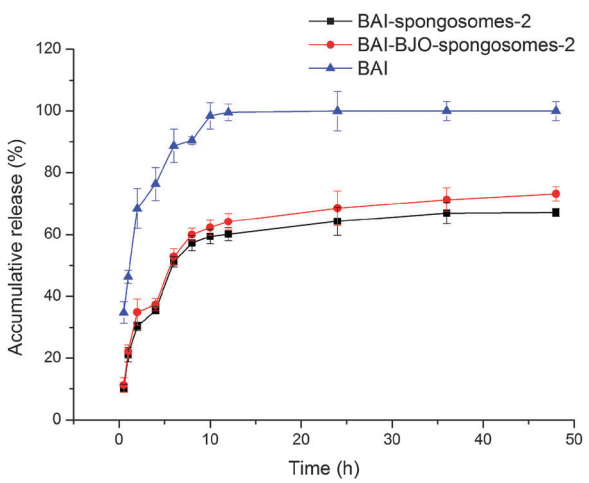

Fig. 5 Cumulative *in vitro* release of the BAI drug from suspension or from BAI-loaded and BAI-BJO-loaded spongosomes in PBS release medium (pH 7.4) at 37 °C. All values are expressed as mean values ± SD (n = 3).

of BJO does not modify the release rate behavior of BAI from the channel system of the multicompartment nanocarriers.

Biological evaluation in cell culture experiments

Fig. 6 presents the cytotoxicity of the investigated spongosome drug delivery nanosystems as evaluated in human lung carcinoma cell line A549. The obtained data show that the BAI-BJO-spongosome-2 nanosystem possesses the highest inhibition potential from all formulations studied in the concentration range of 15 to 120 μg mL^{-1}. This implies that the multidrug-loaded carriers appear to be more efficient in their anti-cancer apoptotic effect in comparison to the single-drug formulations. Indeed, the results summarized in Table 2 indicate that multidrug spongosome carriers (BAI-BJO-spongosome-2) display approximately 2.1 times lower IC_{50} value in comparison to that of the single-BAI spongosome particles (BAI-spongosome-2) and 3.4 times lower than that of the free drug (BAI) suspension. These data evidenced that the multidrug-loaded spongosomes are more efficient than either of the single BAI drug-loaded spongosomes or the free BAI drug suspension (Table 3).

The performed apoptotic study determined the initial cell death[35a] occurring with A549 cancer cells exposed to spongosome-encapsulating nanodrugs (Fig. 7 and 8). After incubation with the spongosomes, the human cancer cells were stained without fixation using the DNA-specific fluorescent dye Hoechst 33342, which is suitable for analysis of living cells undergoing early apoptosis.[35a]

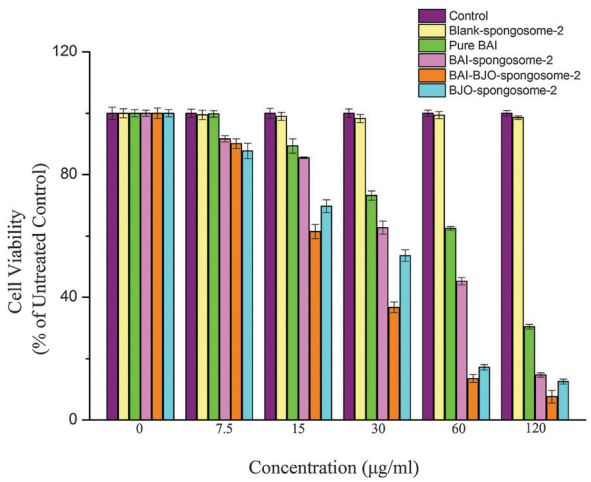

Fig. 6 *In vitro* cytotoxicity of spongosome nanodrug carriers determined with A549 human lung carcinoma cells after exposure of 72 h. The cellular viability is expressed as the percentage of untreated controls. The data are given as mean values ± SD (n = 6).

Table 3 IC_{50} values for spongosome nanodrug carriers determined by MTT assay with A549 human lung carcinoma cells

Treatment group	IC50 (μg mL^{-1}) (n = 3)
Pure BAI	73.2 ± 2.5
BAI-spongosome-2	45.9 ± 3.1
BAI-BJO-spongosome-2	21.4 ± 1.2
BJO-spongosome-2	28.1 ± 3.3
Blank-spongosome-2	>5000

It will be useful to recall that apoptosis involves characteristic cellular morphology changes (cell shrinkage), chromatin condensation, cytoplasm vacuolization, mitochondrial degradation, DNA fragmentation, and cellular breakdown into apoptotic bodies.[35b] The present work established that the A549 cell spheroids are intact in the control sample (Fig. 7A). At variance, the drug-treated A549 cancer cells displayed bright staining (red arrows in Fig. 8), which is characteristic of chromatin condensation associated with apoptosis. There was marginal evidence for apoptotic bodies in the cancer cell population when it was treated with the free BAI drug suspension characterized by low bioavailability (Fig. 7C). Apoptotic bodies (red circles) and DNA fragmentation were readily visible for the multidrug nanoformulation treatment (Fig. 7E). Less brightly stained cells were observed with the single drug-loaded, spongosome-treated groups (Fig. 7D and F).

The possible synergistic effect exerted by the two drugs encapsulated in spongosome nanocarriers was considered through the following formula:[36]

$$\mathrm{CI} = \frac{C_{\mathrm{A},x}}{\mathrm{IC}_{x,\mathrm{A}}} + \frac{C_{\mathrm{B},x}}{\mathrm{IC}_{x,\mathrm{B}}}$$

where $C_{A,x}$ and $C_{B,x}$ are the concentrations of the drugs A and B used in a combination in order to achieve x% drug effect, and $IC_{x,A}$ and $IC_{x,B}$ are the concentrations for the single therapeutic agents to achieve the same effect. Values of CI of less than 1, equal to 1, and higher than 1 would correspond to drug synergy, drug additivity, and drug antagonism, respectively.[36]

In the present case, the IC_{50} values of BAI and BJO were 31.3 μg mL^{-1} ($C_{50,A}$) and 20.7 μg mL^{-1} ($C_{50,B}$) when used in combination. The IC_{50} values of BAI and BJO were 73.2 μg mL^{-1} ($IC_{50,A}$) and 68.5 μg mL^{-1} ($IC_{50,B}$) when the drugs were separately used. The estimated value for CI equal to 0.73 (*i.e.* effectively CI less than 1) provides a theoretical proof for the synergistic drug effect achieved through the multidrug encapsulation in sterically stabilized, multicompartment nanosponge-type carriers.

Discussion

The proposed self-assembly fabrication nanotechnology for multidrug delivery carriers benefits from the advantages of both anticancer agents (BAI and BJO) co-encapsulated in nanoscale objects and exerting the established synergistic effect. Regarding the mechanism of nanoparticle performance and nanodrug action at the intracellular level, diverse signaling pathways may be envisioned to explain the synergistic activity achieved with the multidrug delivery system in human lung carcinoma cells. It is expected that nanoparticles loaded by BAI may suppress the cell cycle progression and induce cell apoptosis.[29b] Gao *et al.*[30c] have suggested that baicalin cytotoxicity to lung cancer cells is mainly due to alteration of the cell cycle and the induction of apoptosis through regulation of the expression of cyclin proteins p53 and Bax. Zhang *et al.*[29c] have supposed that the inhibition of PGE_2 synthesis *via* suppression of COX-2 expression in head and neck squamous cell carcinoma (HNSCC) could be responsible for the anticancer activity of *Scutellaria baicalensis*. Liu *et al.*[30b] have shown that baicalin can induce apoptosis in cells deficient in

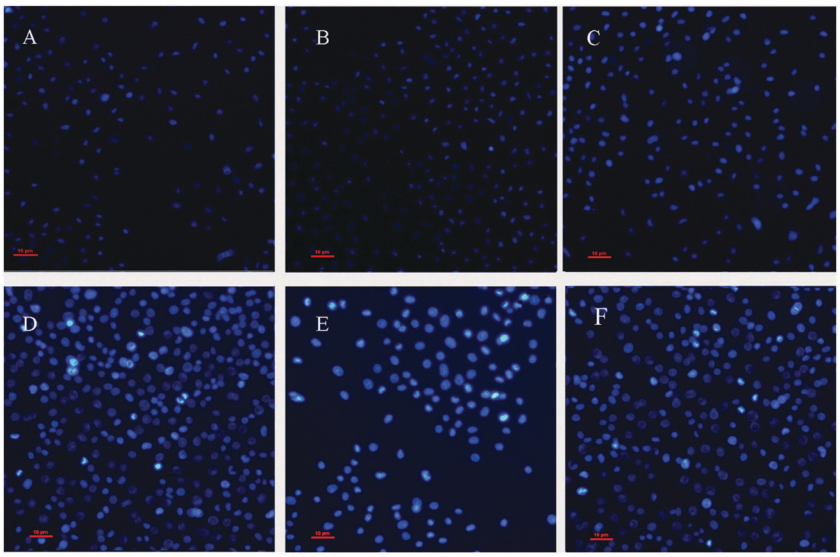

Fig. 7 Effect of different treatments on apoptosis of human lung carcinoma A549 cells: (A) control cells with no treatment; cells treated with (B) blank-spongosomes-2, (C) single-drug BAI suspension, (D) BAI-spongosomes-2, (E) BAI-BJO-spongosomes-2, and (F) BJO-spongosomes-2. The concentration of BAI is 20 μg mL^{-1} in the nanoformulations.

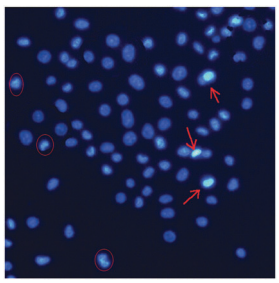

Fig. 8 Magnified presentation of the image from Fig. 7E. The bright patterns (indicated by red arrows and circles) highlight the chromatin condensation associated with cancer cell apoptosis.

MMR genes. For example, baicalin has induced apoptosis in HCT-116 colorectal cancer cells (loss of *hMLH1*) and LoVo cells (loss of *hMSH2*).[30b]

At the same time, *Brucea javanica* can inhibit cell proliferation by regulation of the cell cycle and morphology, controlling the apoptotic gene expression and altering the process of cellular immunity.[30d] Zhang *et al.*[31a] have demonstrated that *Brucea javanica* oil can induce cell apoptosis in human acute myeloid leukemia cell line by activation of caspase-8 and modulation of apoptosis-related proteins. The resistance index of cancer cells was dramatically decreased when drug-resistant ovarian cancer cells were exposed to *Brucea javanica* oil emulsion.[27c]

Considering the low bioavailability of the weakly soluble BAI and BJO phytochemical agents, delivery systems have been required for either of these drugs in chemotherapy trials. For instance, Hao *et al.*[31b] have reported BAI-loaded solid lipid nanoparticles (SLN) prepared by a coacervation method. The SLN formulation has yielded rather large mean particle sizes (343.7 ± 7.1 nm) at an encapsulation efficiency of 86.3 ± 1.4%. The performed pharmacokinetics study has established that SLN may enhance BAI absorption compared to the free BAI drug suspension. Jin *et al.*[31c] have used a nanocrystal suspension of BAI as a drug delivery system in order to improve its bioavailability. The mean particles size of the baicalin nanocrystals was 236 nm (PDI of 0.173), and the zeta potential value was −34.8 mV. Recently, Wu *et al.*[31a] have prepared liposome delivery systems for BAI, which have displayed a mean particle size of 373 ± 15.5 nm and entrapment efficiency of 82.7 ± 0.6%. Baicalin-loaded micelles have been characterized with a loading capacity of 16.94%, entrapment efficiency of 90.67%, and sustained release properties at a mean particle size of 15.6 ± 0.6 nm.[32a] The transdermal permeability of baicalin has been investigated with a local delivery system created by incorporation of Transcutol P (TP) diethylene glycol monoethyl ether in a glyceryl monooleate (GMO)-based cubic phase gel.[32a]

BJO has been previously administered as a therapeutic component in emulsions for intravenous injection and also though capsules, microcapsules, and oral emulsions. However, BJO emulsions have been thermodynamically unstable, which is associated with phase separation events. To solubilize BJO, Yang *et al.*[32c] have prepared an oil-in-water (o/w) microemulsion consisting of Solutol HS 15, sorbitol and IPM. This system has been more stable compared to traditional emulsions. Liposomes have been investigated as a potential BJO delivery system in anti-tumor therapy. BJO-loaded liposomes[25a] have displayed an average diameter of 108.2 nm, a zeta potential of −57.0 mV and drug loading of 3.60. Recent studies have suggested possible synergistic effects of BJO emulsions with certain anticancer drugs (*e.g.* docetaxel)[25c] and coix seed oil.[32d] The synergistic effect observed here of BAI and BJO, encapsulated in a controlled release nanosystem, seems to be more advantageous as compared to previously studied BJO emulsions.

Our work proposes sterically stabilized PEGylated spongosome nanocarriers with controlled release properties. The results obtained here evidence that the creation of multidrug delivery

nanocarriers of mesocrystalline nature, through the combination of baicalin (BAI) and *Brucea javanica* oil (BJO) in nanoassemblies, provides superior characteristics compared to the reported monodrug therapeutic formulations. The sponge nanoorganization favors high encapsulation of compounds of varying hydrophobicity/hydrophilicity and solubility, which has not been possible with classical micellar and liposomal carriers. Whereas micelles, emulsions and SLN can mainly solubilize the oil-type therapeutic agent (BJO), unilamellar liposomes may be more appropriate for the entrapment of the partially hydrophilic drug (BAI) but cannot reach high loading of BJO. Moreover, the possibility to target multiple intracellular signaling pathways *via* synergistic nanodrug action, offered by the concept of alternative anticancer therapies *via* nanosponge medicines, enabled the enhanced suppression of cancer cell proliferation and the induction of apoptosis. This proves the unique properties of the nanosponge drug carriers designed here, which ensured sustained drug release in the cancer cell model.

Conclusion

Sterically stabilized, bicontinuous sponge nanoparticles encapsulating a combination of anticancer agents (BAI and BJO) were produced by self-assembly mixtures of biocompatible building blocks comprised by glycerol monooleate, Polysorbate 80, and sodium alginate. The tunable properties of the inner aqueous and lipophilic compartments of the nanocarriers were assessed by high-resolution structural investigations. The choice of the drugs, co-encapsulated in the mesocrystalline systems, was determined by the necessity to combine bioactive substances with adjoining therapeutic effects in each nanocarrier object. Thus, the anticancer drug baicalin was co-delivered with the safety component BJO, characterized by broad biological activity and aiming at reduced side effects of the nanodrug formulation as well as organ preservation. The combination of the two drugs considerably increased the number of apoptotic cancer cells upon *in vitro* administration. The synergy of the multidrug delivery system is associated with enhanced action of the co-encapsulated drugs compared to the monotherapy approach. Therefore, the designed PEGylated lipid nanosponges represent a new functional material of multicompartment organization (permitting encapsulation of both hydrophobic and hydrophilic therapeutic agents) that provides controlled release profiles and long-term stability of the loaded nanodrugs. In perspective, the sequential release and pharmacokinetics of the multidrug nanosponge carriers may be *in vivo* evaluated toward translation to clinical examinations. Multidrug delivery is currently desired for the treatment of lung, ovarian, and gastrointestinal cancers.

Experimental section

1 Chemicals and materials

Baicalin (BAI 95%, Aladdin Chemical Reagent Co. Ltd, China), *Brucea javanica* seed oil (BJO, 63.3% oleic acid, a gift from Yan'an Changtai Pharmaceutical Co., Ltd, China), Polysorbate (P80, Sigma-Aldrich, MO, USA), alginic acid sodium salt (alginate, Sigma-Aldrich, MO, USA), glycerol monooleate (MO, 99%, General-Reagent Co. Ltd, China), 3-(4,5-dimethylthiazol-2-yl)-2,5-diphenyltetrazolium bromide (MTT 98%, Sigma-Aldrich, MO, USA), and Hoechst 33342 (Beyotime Biotechnology Co. China) were used as received. MilliQ filtered water (resistivity 18.2 MΩ cm, Millipore Co.) was used for preparation of the aqueous phases (PBS, baicalin solution, *etc.*).

2 Sample preparation

Liquid crystalline nanoparticles (spongosomes) were fabricated by hydration of a dry lipid film followed by physical agitation (Table 1). Agitation steps of vortexing, ice bath sonication, and high-pressure homogenization (HPH) were performed in a scheme of sequential cycles. Briefly, the MO and P80 were dissolved in chloroform and placed in 50 mL pear-shaped flasks. The mixtures were subjected to rotary evaporation, and the residual organic solvent was further dried under vacuum at room temperature overnight. The lipid films were hydrated with appropriate volumes of buffer solution (PBS pH 7.4, 0.5 wt% sodium alginate) for 1 hour by applying vortex shaking every 10 minutes at room temperature. The dispersions were further stirred intensely at 10 000 rmp for 1 min. For blank-spongosome-1 nanoparticle preparation, the dispersions were first processed through a high-pressured homogenizer (HPH ATS Engineering, Canada) with five homogenization cycles at 850 bar, before sonication in ice bath for 15 min (agitation method 1). For blank-spongosomes-2 particle preparation, the physical agitation sequence was performed in the reversed order, *i.e.* the dispersion went through HPH (5 cycles) after sonication in ice bath for 15 min (agitation method 2). BAI-loaded spongosomes were prepared by the same procedures (method 1 and method 2), except the lipid film was initially hydrated in a buffer solution of BAI (PBS pH 7.4, 0.5 wt% sodium alginate). For the multidrug-loaded spongosome preparations, the lipophilic oil component BJO was added in the chloroform solution used for the thin lipid film preparation. The sample dispersion and homogenization methods were identical for the blank and BAI-loaded nanocarriers.

3 Dynamic light scattering and zeta potential measurements

Dynamic light scattering (DLS) was employed for determination of the mean particle sizes, particle distributions, and zeta potentials of freshly prepared samples. The Delsa™ Nano C Particle Analyzer (Beckman Coulter, USA) was operated at a fixed angle of 165° and at 25 °C. Each measurement was repeated three times.

4 Entrapment efficiency and drug loading in nanocarriers

The ultrafiltration centrifugal method was used to assess the entrapment efficiency (EE) of baicalin in the spongosome nanocarriers. The free drug concentration in the samples after centrifugation and supernatant collection was determined by the UV-vis spectrophotometric method. An aliquot (2 mL) of the dispersion was placed in the upper chamber of a centrifuge tube, matched with an ultrafilter of MWCO = 10 kDa (Amicon® Ultra-4 Centrifugal Filter Units, Millipore, USA). The sample was centrifuged for 15 min at 9500 rpm at 4 °C in order to

separate the particles from the aqueous phase. Subsequently, the aqueous phase was diluted in PBS (pH 7.4), and the absorption was measured at a wavelength 315 nm by means of a UV-vis spectrophotometer (UV-1800, Shimadzu, Japan). The calibration curve of absorption (Abs) *versus* baicalin concentration (C) was plotted as Abs = $0.0424C + 0.0069$ ($R^2 = 0.9999$). All experiments were performed at room temperature (25 °C).

The drug loading (DL%) and the entrapment efficiency (EE%) were determined using the following formulae:

$$\mathrm{EE}\% = \left(1 - \frac{C_\mathrm{U}}{C_\mathrm{T}}\right) \times 100\%$$

$$\mathrm{DL}\% = \left(\frac{C_\mathrm{T} - C_\mathrm{U}}{C_\mathrm{L}}\right) \times 100\%$$

where C_U is the amount of non-entrapped BAI (free unloaded drug), C_T is the total amount of BAI added to the dispersion system, and C_L is the total lipid amount.

5 Small-angle X-ray scattering (SAXS)

Small-angle X-ray diffraction and scattering experiments (SAXS) were performed using a pinhole camera (Molecular Metrology SAXS System) connected to a microfocused X-ray beam generator (Bede, Durham, UK) operated at 45 kV and 0.66 mA (30 W). The camera was equipped with a multiwire, gas-filled area detector with an active area diameter of 20 cm and 512 × 512 pixels (Gabriel design). An X-ray diode was installed as a beamstop in the center of the detector. Measurements were performed in a momentum transfer range of $4.610^{-3} < q < 0.19$ Å^{-1} (wavelength $\lambda = 1.54$ Å^{-1}).

6 Cryogenic transmission electron microscopy (Cryo-TEM)

For cryo-transmission electron microscopy studies, a sample droplet of 2 μL was placed on a lacey carbon-filmed copper grid (Science Services, Muenchen), which was hydrophilized by air plasma glow discharge (Solarus 950, Gatan, Muenchen, Germany) for 30 s. Subsequently, most of the liquid was removed with blotting paper, leaving a thin film stretched over the lace holes. The specimens were instantly shock-frozen by rapid immersion into liquid ethane, cooled to approximately 90 K by liquid nitrogen in a temperature-controlled freezing unit (Zeiss Cryobox, Carl Zeiss Microscopy GmbH, Jena, Germany). The temperature was monitored and kept constant in the chamber during all the sample preparation steps. After freezing the specimens, the remaining ethane was removed using blotting paper. The specimen was inserted into a cryo transfer holder (CT3500, Gatan, Muenchen, Germany) and transferred to a Zeiss/Leo EM922 Omega EFTEM (Zeiss Microscopy GmbH, Jena, Germany). Examinations were carried out at temperatures around 90 K. The TEM was operated at an acceleration voltage of 200 kV. Zero-loss filtered images (ΔE = 0 eV) were taken under reduced dose conditions (100–1000 e nm^{-2}). All images were registered digitally by a bottom-mounted CCD camera system (Ultrascan 1000, Gatan, Muenchen, Germany), combined and processed with a digital imaging processing system (Digital Micrograph GMS 1.9, Gatan, Muenchen, Germany).

7 *In vitro* baicalin release studies

The *in vitro* release of baicalin from spongosome nanocarriers was investigated by the dialysis method. Freshly prepared samples (3 mL) were placed in a dialysis tube (MWCO = 14 kDa). The latter was incubated in 150 mL of release medium (PBS, pH = 7.4) at 37 °C under rotary shaking. Samples (4 mL) were taken out from the release medium at predetermined time intervals, and the system was refilled with the same volume of fresh medium. Baicalin content was determined by UV-vis spectrophotometer (UV-1800, Shimadzu, Japan) at a wavelength of 315 nm. All experiments were performed in triplicate.

8 Cell culture experiments

The human lung carcinoma cell line A549 was purchased from the American Type Culture Collection (ATCC CCL-185, Manassas, VA, USA). The A549 cells (*Homo sapiens*) were cultured in cell culture dishes containing PRMI-1640 medium supplemented with 10% fetal bovine serum (Gibco, Grand Island, NY, USA) and penicillin (100 U mL^{-1}) at 37 °C in a humidified 5% CO_2 atmosphere.

9 *In vitro* cytotoxicity assay

Cell viability was measured by 3-(4,5-dimethylthiazol-2-yl)-2,5-diphenyltetrazolium bromide (MTT) assay. Its principle is based on the determination of enzymatic metabolic activity through the reduction of MTT (yellow color) to an insoluble formazan product (dark purple color) by the mitochondrial succinate dehydrogenase. MTT stock solution was prepared in PBS at 5 mg mL^{-1} concentration and subsequently filtered through a 0.2 μm filter (Sartorius). The A549 cells were seeded in 96-well plates at a density of 5×10^3 cells per well, containing 200 μL medium. After 24 h, the growth medium was removed, the cells were washed and exposed to various concentrations of blank-spongosomes-2, free drug BAI, BAI-spongosomes-2, BAI-BJO-spongosomes-2 and BJO-spongosomes-2, dispersed in medium with no fetal bovine serum. After 72 h cell exposure to nanoparticles in the lack of serum, 20 μL MTT solution (5 mg mL^{-1}) was directly added into each well and incubated for a fixed period between 1 and 4 h at 37 °C. The resulting formazan crystals were solubilized with 200 μL DMSO. For formazan quantification, the absorbance was measured using an enzyme-linked immunosorbent microplate assay reader at 570 nm. The effect of the nanoparticle formulations on cell proliferation was expressed as the cell viability percentage. Untreated cells were considered as 100% viable.

10 Cell apoptosis assay

The A549 cancer cells were seeded into 24-well plates at a density of 1×10^4 cells per well. After 24 h of incubation, the A549 cells were exposed to blank-spongosomes-2, free drug BAI, BAI-spongosomes-2, BAI-BJO-spongosomes-2 and BJO-spongosomes-2 (20 μg mL^{-1} of BAI) for 72 h. Then, the cells were washed with cold PBS buffer. A solution of Hoechst 33342 (5 μg mL^{-1}) was added and incubated for 15 min at room temperature. The unreacted Hoechst dye was removed by cold

PBS buffer (2 × 1 mL washes). To examine the degree of cell apoptosis, the stained cells were analyzed under a fluorescent microscope (ECLIPSE Ti-S, Nikon, Japan).

Acknowledgements

A.Z. and Y.C. thank the Shanghai Natural Science Foundation (K100-2-15017), the National Natural Science Foundation of China (No. 21573070), Fundamental Research Funds for the Central Universities and Alexander von Humboldt Foundation for financial support. B.A. thanks the Czech Science Foundation (Grant No. GACR 15-10527J) and M.D. thanks BIMF (Bayreuth Institute of Macromolecular Research) and BZKG (Bayreuth Center for Colloids and Interfaces) for financial support.

References

1 (*a*) C. Nilsson, J. Østergaard, S. W. Larsen, C. Larsen, A. Urtti and A. Yaghmur, *Langmuir*, 2014, **30**, 6398–6407; (*b*) X. Mulet, B. J. Boyd and C. J. Drummond, *J. Colloid Interface Sci.*, 2013, **393**, 1–20; (*c*) B. Angelov, A. Angelova, S. K. Filippov, M. Drechsler, P. Štěpánek and S. Lesieur, *ACS Nano*, 2014, **8**, 5216–5226; (*d*) B. Angelov, A. Angelova, S. K. Filippov, G. Karlsson, N. Terrill, S. Lesieur and P. Štěpánek, *Soft Matter*, 2011, **7**, 9714–9720.

2 (*a*) M. Wadsater, J. Barauskas, T. Nylander and F. Tiberg, *ACS Appl. Mater. Interfaces*, 2014, **6**, 7063–7069; (*b*) A. Angelova, B. Angelov, R. Mutafchieva, S. Lesieur and P. Couvreur, *Acc. Chem. Res.*, 2011, **44**, 147–156; (*c*) A. Angelova, B. Angelov, R. Mutafchieva and S. Lesieur, *J. Inorg. Organomet. Polym. Mater.*, 2015, **25**, 214–232.

3 (*a*) A. Zabara and R. Mezzenga, *J. Controlled Release*, 2014, **188**, 31–43; (*b*) B. Angelov, A. Angelova, S. K. Filippov, T. Narayanan, M. Drechsler, P. Štěpánek, P. Couvreur and S. Lesieur, *J. Phys. Chem. Lett.*, 2013, **4**, 1959–1964; (*c*) A. Angelova, B. Angelov, M. Drechsler and S. Lesieur, *Drug Discovery Today*, 2013, **18**, 1263–1271.

4 (*a*) A. Gupta, T. Stait-Gardner, L. de Campo, L. J. Waddington, N. Kirby, W. S. Price and M. J. Moghaddam, *J. Mater. Chem. B*, 2014, **2**, 1225–1233; (*b*) A. Angelova, B. Angelov, B. Papahadjopoulos-Sternberg, C. Bourgaux and P. Couvreur, *J. Phys. Chem. B*, 2005, **109**, 3089–3093; (*c*) A. Angelova, B. Angelov, M. Drechsler, V. M. Garamus and S. Lesieur, *Int. J. Pharm.*, 2013, **454**, 625–632; (*d*) I. Martiel, S. Handschin, W. K. Fong, L. Sagalowicz and R. Mezzenga, *Langmuir*, 2015, **31**, 96–104.

5 (*a*) S. F. Hedegaard, C. Nilsson, P. Laurinmaki, S. Butcher, A. Urtti and A. Yaghmur, *RSC Adv.*, 2013, **3**, 24576–24585; (*b*) B. Angelov, A. Angelova, B. Papahadjopoulos-Sternberg, S. V. Hoffmann, V. Nicolas and S. Lesieur, *J. Phys. Chem. B*, 2012, **116**, 7676–7686; (*c*) L. N. Borgheti-Cardoso, L. V. Depieri, H. Diniz, M. C. de Abreu Fantini, M. M. Iyomasa, F. T. Moura de Carvalho Vicentini and M. V. Bentley, *Eur. J. Pharm. Sci.*, 2014, **58**, 72–82; (*d*) H. H. Shen, V. Lake, A. P. Le Brun, M. James, A. P. Duff, Y. Peng, K. M. McLean and P. G. Hartley, *Biomaterials*, 2013, **34**, 8361–8369.

6 (*a*) M. Rappolt, G. M. Di Gregorio, M. Almgren, H. Amenitsch, G. Pabst, P. Laggner and P. Mariani, *Europhys. Lett.*, 2006, **75**, 267–273; (*b*) A. Angelova, B. Angelov, B. Papahadjopoulos-Sternberg, M. Ollivon and C. Bourgaux, *J. Drug Delivery Sci. Technol.*, 2005, **15**, 108–112; (*c*) B. Angelov, A. Angelova, V. M. Garamus, M. Drechsler, R. Willumeit, R. Mutafchieva, P. Štěpánek and S. Lesieur, *Langmuir*, 2012, **28**, 16647–16655.

7 (*a*) A. Yaghmur, P. Laggner, M. Almgren and M. Rappolt, *PLoS One*, 2008, **3**, e3747; (*b*) B. Angelov, A. Angelova, R. Mutafchieva, S. Lesieur, U. Vainio, V. M. Garamus, G. V. Jensen and J. S. Pedersen, *Phys. Chem. Chem. Phys.*, 2011, **13**, 3073–3081.

8 (*a*) A. Yaghmur, B. Sartori and M. Rappolt, *Phys. Chem. Chem. Phys.*, 2011, **13**, 3115–3125; (*b*) A. Angelova, B. Angelov, V. M. Garamus, P. Couvreur and S. Lesieur, *J. Phys. Chem. Lett.*, 2012, **3**, 445–457; (*c*) B. Angelov, A. Angelova, M. Ollivon, C. Bourgaux and J. Campitelli, *J. Am. Chem. Soc.*, 2003, **125**, 7188–7189.

9 A. W. Dong, C. Fong, L. J. Waddington, A. J. Hill, B. Boyd and C. J. Drummond, *Phys. Chem. Chem. Phys.*, 2015, **17**, 1705–1715.

10 (*a*) E. Esposito, P. Mariani, L. Ravani, C. Contado, M. Volta, S. Bido, M. Drechsler, S. Mazzoni, E. Menegatti, M. Morari and R. Cortesi, *Eur. J. Pharm. Biopharm.*, 2012, **80**, 306–314; (*b*) B. Angelov, A. Angelova, M. Drechsler, V. M. Garamus, R. Mutafchieva and S. Lesieur, *Soft Matter*, 2015, **11**, 3686–3692; (*c*) E. Esposito, L. Ravani, P. Mariani, N. Huang, P. Boldrini, M. Drechsler, G. Valacchi, R. Cortesi and C. Puglia, *Eur. J. Pharm. Biopharm.*, 2014, **86**, 121–132; (*d*) S. Deshpande, E. Venugopal, S. Ramagiri, J. R. Bellare, G. Kumaraswamy and N. Singh, *ACS Appl. Mater. Interfaces*, 2014, **6**, 17126–17133.

11 (*a*) R. Cortesi, L. Ravani, E. Menegatti, M. Drechsler and E. Esposito, *Indian J. Pharm. Sci.*, 2011, **73**, 687–693; (*b*) E. Esposito, L. Ravani, C. Contado, A. Costenaro, M. Drechsler, D. Rossi, E. Menegatti, A. Grandini and R. Cortesi, *Mater. Sci. Eng., C*, 2013, **33**, 411–418; (*c*) A. M. Avachat and S. S. Parpani, *Colloids Surf., B*, 2014, **126**, 87–97; (*d*) M. Cohen-Avrahami, A. I. Shames, M. F. Ottaviani, A. Aserin and N. Garti, *Colloids Surf., B*, 2014, **122**, 231–240.

12 (*a*) T. H. Nguyen, T. Hanley, C. J. Poter and B. J. Boyd, *J. Controlled Release*, 2011, **153**, 180–186; (*b*) N. Bye, O. E. Hutt, T. M. Hinton, D. P. Acharya, L. J. Waddington, B. A. Moffat, D. K. Wright, H. X. Wang, X. Multe and B. W. Muir, *Langmuir*, 2014, **30**, 8898–8906; (*c*) C. Souza, E. Watanabe, L. N. Borgheti-Cardoso, M. C. De Abreu Fantini and M. G. Lara, *J. Pharm. Sci.*, 2014, **103**, 3914–3923.

13 (*a*) M. Komisarski, Y. M. Osornio, J. S. Siegel and E. M. Landau, *Chem. – Eur. J.*, 2013, **19**, 1262–1267; (*b*) E. A. Estracanholli, F. S. Praca, A. B. Cintra, M. B. Pierre and M. G. Lara, *AAPS PharmSciTech*, 2014, **15**, 1468–1475; (*c*) E. Esposito, R. Cortesi, M. Drechsler, L. Paccamiccio,

P. Mariani, C. Contado, E. Stellin, E. Menegatti, F. Bonina and C. Puglia, *Pharm. Res.*, 2005, **22**, 2163–2173; (*d*) P. Verma and M. Ahuja, *Int. J. Biol. Macromol.*, 2015, **73**, 138–145.

14 (*a*) S. B. Rizwan, W. T. McBurney, K. Young, T. Hanley, B. J. Boyd, T. Rades and S. Hook, *J. Controlled Release*, 2013, **165**, 16–21; (*b*) R. Petrilli, F. S. G. Praca, A. R. H. Carollo, W. S. G. Medina, K. T. de Oliveira, M. C. A. Fantini, M. D. G. P. M. S. Neves, J. A. S. Cavaleiro, O. A. Serra, Y. Lamamoto and M. V. L. B. Bentley, *Curr. Nanosci.*, 2013, **9**, 434–441; (*c*) M. Salim, H. Minamikawa, A. Sugimura and R. Hashim, *Med. Chem. Commun.*, 2014, **5**, 1602–1618; (*d*) W. Wu, J. Li, L. Wu, B. Wang, Z. Wang, Q. Xu and H. Xin, *AAPS PharmSciTech*, 2013, **14**, 1063–1071.

15 (*a*) E. Nazaruk, M. Szlezak, E. Gorecka, R. Bilewicz, Y. M. Osornio, P. Uebelhart and E. M. Landau, *Langmuir*, 2014, **30**, 1383–1390; (*b*) A. Angelova, C. Ringard-Lefebvre and A. Baszkin, *J. Colloid Interface Sci.*, 1999, **212**, 275–279; (*c*) A. Angelova, J. Reiche, R. Ionov, D. Janietz and L. Brehmer, *Thin Solid Films*, 1994, **242**, 289–294; (*d*) T. A. Balbino, A. A. Gasperini, C. L. Oliveira, A. R. Azzoni, L. P. Cavalcanti and L. G. de La Torre, *Langmuir*, 2012, **28**, 11535–11545.

16 (*a*) A. Zabara, R. Negrini, O. Onaca-Fischer and R. Mezzenga, *Small*, 2013, **9**, 3602–3609; (*b*) A. Angelova, F. Penacorada, B. Stiller, T. Zetzsche, R. Ionov, H. Kamusewitz and L. Brehmer, *J. Phys. Chem.*, 1994, **98**, 6790–6796; (*c*) A. Angelova, C. Ringard-Lefebvre and A. Baszkin, *J. Colloid Interface Sci.*, 1999, **212**, 280–285; (*d*) T. Kojarunchitt, S. Baldursdottir, Y. D. Dong, B. Boyd, T. Rades and S. Hook, *Eur. J. Pharm. Biopharm.*, 2015, **89**, 74–81.

17 (*a*) A. Zabara and R. Mezzenga, *Soft Matter*, 2012, **8**, 6535–6541; (*b*) J. G. Petrov and A. Angelova, *Langmuir*, 1992, **8**, 3109–3115; (*c*) N. Rahanyan-Kaegi, S. Aleandri, C. Speziale, R. Mezzenga and E. M. Landau, *Chem. – Eur. J.*, 2015, **21**, 1873–1877.

18 (*a*) J. Barauskas, L. Christerson, M. Wadsäter, F. Lindström, A. K. Lindqvist and F. Tiberg, *Mol. Pharmaceutics*, 2014, **11**, 895–903; (*b*) J. G. Petrov, A. Angelova and D. Mobius, *Langmuir*, 1992, **8**, 206–212; (*c*) T. E. Hartnett, K. Ladewig, A. J. O'Connor, P. G. Hartley and K. M. McLean, *RSC Adv.*, 2015, **3**, 26543–26549.

19 (*a*) H. M. Barriga, A. I. Tyler, N. L. McCarthy, E. S. Parsons, O. Ces, R. V. Law, J. M. Seddon and N. J. Brooks, *Soft Matter*, 2015, **11**, 600–607; (*b*) J. G. Petrov, D. Mobius and A. Angelova, *Langmuir*, 1992, **8**, 201–205; (*c*) M. Cano-Sarabia, A. Angelova, N. Ventosa, S. Lesieur and J. Vecina, *J. Colloid Interface Sci.*, 2010, **350**, 10–15.

20 (*a*) V. Jain, N. K. Swarnakar, P. R. Mishra, A. Verma, A. K. Mishra and N. K. Jain, *Biomaterials*, 2012, **33**, 7206–7220; (*b*) H. Richly, B. Schultheis, I. A. Adamietz, P. Kupsch, M. Grubert, R. A. Hilger, M. Ludwig, E. Brendel, O. Christensen and D. Strumberg, *Eur. J. Cancer*, 2009, **45**, 579–587; (*c*) L. Cai, G. Xu, C. Shi, D. Guo, X. Wang and J. Luo, *Biomaterials*, 2015, **37**, 456–468; (*d*) Y. Mi, J. Zhao and S. S. Feng, *J. Controlled Release*, 2013, **169**, 185–192.

21 (*a*) S. M. Sagnella, X. Gong, M. J. Moghaddam, C. E. Conn, K. Kimpton, L. J. Waddington, I. Krodkiewska and C. J. Drummond, *Nanoscale*, 2011, **3**, 919–924; (*b*) E. Markovsky, H. Baabur-Cohen and R. Satchi-Fainaro, *J. Controlled Release*, 2014, **187**, 145–157; (*c*) G. P. Mishra, D. Nguyen and A. W. Alani, *Mol. Pharmaceutics*, 2013, **10**, 2071–2078; (*d*) N. K. Swarnakar, K. Thanki and S. Jain, *Nanomedicine*, 2014, **10**, 1231–1241.

22 (*a*) D. F. Zhou, Y. W. Cong, Y. X. Qi, S. S. He, H. J. Xiong, Y. J. Wu, Z. G. Xie, X. S. Chen, X. B. Jing and Y. B. Huang, *Biomater. Sci.*, 2015, **3**, 182–191; (*b*) S. Mignani, M. Bryszewska, B. Klajnert-Maculewicz, M. Zablocka and J. P. Majoral, *Biomacromolecules*, 2015, **16**, 1–27; (*c*) M. Milczarek, M. Psurski, A. Kutner and J. Wietrzyk, *BMC Cancer*, 2013, **13**, 294; (*d*) A. Avan, K. Quint, F. Nicolini, A. E. Frampton, M. Maftouh, S. Pelliccioni, G. J. Schuurhuis, G. J. Peters and E. Giovannetti, *Curr. Pharm. Des.*, 2013, **19**, 940–950.

23 (*a*) T. Y. Jiang, R. Mo, A. Bellotti, J. P. Zhou and G. Zhen, *Adv. Funct. Mater.*, 2014, **24**, 2295–2304; (*b*) V. Gupta, K. Chuttani, A. K. Mishra and P. Trivedi, *J. Labelled Compd. Radiopharm.*, 2014, **57**, 425–433; (*c*) N. K. Swarnakar, K. Thanki and S. Jain, *Pharm. Res.*, 2014, **31**, 1219–1238; (*d*) F. Zhao, H. Yin and J. Li, *Biomaterials*, 2014, **35**, 1050–1062.

24 (*a*) T. Liu, W. Xue, B. Ke, M. Q. Xie and M. Dong, *Biomaterials*, 2014, **35**, 3865–3872; (*b*) C. Kim, B. P. Shah, P. Subramaniam and K. B. Lee, *Mol. Pharmaceutics*, 2011, **8**, 1955–1961; (*c*) S. Sreenivasan and S. Krishnakumar, *Curr. Eye Res.*, 2014, **12**, 1–13; (*d*) Y. D. Wen, Y. L. Ho, R. J. Shiau, J. K. Yeh, J. Y. Wu, W. L. Wang and S. J. Chiou, *J. Organomet. Chem.*, 2010, **695**, 352–359; (*e*) T. Liu, M. Wang, T. Wang, Y. Yao and N. Zhang, *Colloids Surf., B*, 2015, **126**, 531–540.

25 (*a*) Y. Cui, Z. Wu, X. Liu, R. Ni, X. Zhu, L. Ma and J. Liu, *AAPS PharmSciTech*, 2010, **11**, 878–884; (*b*) M. Chen, R. Chen, S. Wang, W. Tan, Y. Hu, X. Peng and Y. Wang, *Int. J. Nanomed.*, 2013, **8**, 85–92; (*c*) S. Ma, F. Chen, X. Ye, Y. Dong, Y. Xue, H. Xu, W. Zhang, S. Song, L. Ai, N. Zhang and W. Pan, *Int. J. Nanomed.*, 2013, **8**, 4045–4052.

26 (*a*) T. Krakauer, B. Q. Li and H. A. Young, *FEBS Lett.*, 2001, **500**, 52–55; (*b*) Y. C. Shen, W. F. Chiou, Y. C. Chou and C. F. Chen, *Eur. J. Pharmacol.*, 2003, **465**, 171–181; (*c*) H. Shi, B. Zhao and W. Xin, *Biochem. Mol. Biol. Int.*, 1995, **35**, 981–994.

27 (*a*) Y. Wang, Y. Li, J. Wu and Q. Shen, *Micro Nano Lett.*, 2012, **7**, 256–261; (*b*) F. J. Han, D. Y. Cai, X. K. Wu, X. L. Di and L. Wang, *Mod. Trends Oncol.*, 2013, **21**, 669–671; (*c*) D. Chen, P. Chen and M. Zhu, *J. Emergency Trad. Chin. Med.*, 2009, **18**, 598–599; (*d*) M. W. Hu, Y. W. Yao and H. Q. Wang, *J. Pract. Oncol.*, 2011, **26**, 306–308.

28 (*a*) S. I. Jang, H. J. Kim, K. M. Hwang, S. J. Jekal, H. O. Pae, B. M. Choi, Y. G. Yun, T. O. Kwon, H. T. Chung and Y. C. Kim, *Immunopharmacol. Immunotoxicol.*, 2003, **25**, 585–594; (*b*) J. Y. Wan, X. Gong, L. Zhang, H. Z. Li, Y. F. Zhou and Q. X. Zhou, *Eur. J. Pharmacol.*, 2008, **587**, 302–308.

29 (*a*) C. A. Gonzalez and E. Riboli, *Nutr. Cancer*, 2006, **56**, 225–231; (*b*) X. F. Xu, B. L. Cai, S. M. Guan, Y. Li, J. Z. Wu,

Y. Wang and B. Liu, *Invest. New Drugs*, 2011, **29**, 637–645; (*c*) D. Y. Zhang, J. Wu, F. Ye, L. Xue, S. Jiang, J. Yi, W. Zhang, H. Wei, M. Sung, W. Wang and X. Li, *Cancer Res.*, 2003, **63**, 4037–4043.

30 (*a*) B. L. Yang, F. Liu and X. F. Liu, *World Chin. J. Digestol.*, 2008, **16**, 2376–2380; (*b*) X. F. Liu, H. Y. Jing and S. Q. Ding, *World Chin. J. Digestol.*, 2007, **15**, 2201–2204; (*c*) J. Gao, W. A. Morgan, A. Sanchez-Medina and O. Corcoran, *Toxicol. Appl. Pharmacol.*, 2011, **254**, 221–228; (*d*) L. H. Yang, W. J. Shi and X. Q. Zhao, *J. Mudanjiang Univ.*, 2010, **31**, 65–67.

31 (*a*) H. Zhang, J. Y. Yang, F. Zhou, L. H. Wang, W. Zhang, S. Sha and C. F. Wu, *J. Evidence-Based Complementary Altern. Med.*, 2011, 965016; (*b*) J. Hao, F. Wang, X. Wang, D. Zhang, Y. Bi, Y. Gao, X. Zhao and Q. Zhang, *Eur. J. Pharm. Sci.*, 2012, **47**, 497–505; (*c*) S. Y. Jin, J. Han, S. X. Jin, Q. Y. Lv, J. X. Bai, H. G. Chen, R. S. Li, W. Wu and H. L. Yuan, *Chin. J. Nat. Med.*, 2014, **12**, 71–80; (*d*) Y. Wei, J. Guo, X. Zheng, J. Wu, Y. Zhou, Y. Yu, Y. Ye, L. Zhang and L. Zhao, *Int. J. Nanomed.*, 2014, **9**, 3623–3630.

32 (*a*) H. Zhang, L. Zhao, L. Chu, X. Han and G. Zhai, *J. Colloid Interface Sci.*, 2014, **434**, 40–47; (*b*) Y. Zhang, K. Zhang, T. Guo, Y. Li, C. Zhu and N. Feng, *Int. J. Pharm.*, 2014, **479**, 219–226; (*c*) F. Yang, X. H. Yu, F. Qiao, L. H. Cheng, G. Chen, X. Long, X. R. Wang, X. L. Li, R. C. Liang and Y. Z. Chen, *Drug Dev. Ind. Pharm.*, 2014, **40**, 266–277; (*d*) Y. L. Yu, Y. Lu, X. Tang and F. D. Cui, *Biol. Pharm. Bull.*, 2008, **31**, 673–680.

33 (*a*) E. Esposito, A. Boschi, L. Ravani, R. Cortesi, M. Drechsler, P. Mariani, S. Moscatelli, C. Contado, G. Di Domenico, C. Nastruzzi, M. Giganti and L. Uccelli, *Eur. J. Pharm. Biopharm.*, 2015, **89**, 145–156; (*b*) N. Kolishetti, S. Dhar, P. M. Valencia, L. Q. Lin, R. Karnik, S. J. Lippard, R. Langer and O. C. Farokhzad, *Proc. Natl. Acad. Sci. U. S. A.*, 2010, **107**, 17939–17944; (*c*) J. V. Natarajan, C. Nugraha, X. W. Ng and S. Venkatraman, *J. Controlled Release*, 2014, **193**, 122–138; (*d*) F. Trotta, C. Dianzani, F. Caldera, B. Mognetti and R. Cavalli, *Expert Opin. Drug Delivery*, 2014, **11**, 931–941.

34 (*a*) A. Maksimenko, M. Alami, F. Zouhiri, J. D. Brion, A. Pruvost, J. Mougin, A. Hamze, T. Boissenot, O. Provot, D. Desmaële and P. Couvreur, *ACS Nano*, 2014, **8**, 2018–2032; (*b*) G. Gopalakrishnan, S. Lepetre, A. Maksimenko, S. Mura, D. Desmaële and P. Couvreur, *Adv. Healthcare Mater.*, 2015, **4**, 1015–1022; (*c*) M. A. Madni, M. Sarfraz, M. Rehman, M. Ahmad, N. Akhtar, S. Ahmad, N. Tahir, S. Ijaz, R. Al-Kassas and R. Löbenberg, *J. Pharm. Pharm. Sci.*, 2014, **17**, 401–426.

35 (*a*) G. Yang, T. Yang, W. Zhang, M. Lu, X. Ma and G. Y. Xiang, *J. Agric. Food Chem.*, 2014, **62**, 2207–2215; (*b*) S. J. Heo, K. N. Kim, W. J. Yoon, C. Oh, A. Affan, Y. J. Lee, H. S. Lee and D. H. Kang, *Food Chem. Toxicol.*, 2011, **49**, 1998–2004.

36 L. Zhao, M. G. Wientjes and J. L. Au, *Clin. Cancer Res.*, 2004, **10**, 7994–8004.

